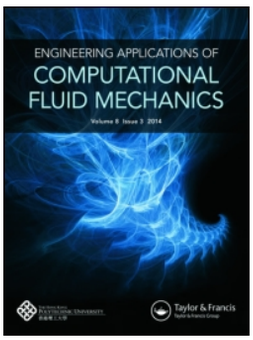

Engineering Applications of Computational Fluid Mechanics

ISSN: 1994-2060 (Print) 1997-003X (Online) Journal homepage: https://www.tandfonline.com/loi/tcfm20

Effect of fan and shroud configurations on underhood flow characteristics of an agricultural tractor

İlhan Öztürk, Cenk Çetin & Mehmet Metin Yavuz

To cite this article: İlhan Öztürk, Cenk Çetin & Mehmet Metin Yavuz (2019) Effect of fan and shroud configurations on underhood flow characteristics of an agricultural tractor, Engineering Applications of Computational Fluid Mechanics, 13:1, 506-518, DOI: 10.1080/19942060.2019.1617192

To link to this article: https://doi.org/10.1080/19942060.2019.1617192

Published online: 03 Jun 2019.

ENGINEERING APPLICATIONS OF COMPUTATIONAL FLUID MECHANICS
2019, VOL. 13, NO. 1, 506–518
https://doi.org/10.1080/19942060.2019.1617192

Taylor & Francis
Taylor & Francis Group

Effect of fan and shroud configurations on underhood flow characteristics of an agricultural tractor

İlhan Öztürk [a,b], Cenk Çetin[c] and Mehmet Metin Yavuz[c]

[a]R&D Department, Türk Traktör ve Ziraat Makinaları A.Ş., Ankara, Turkey; [b]Aerospace Engineering Department, Middle East Technical University, Ankara, Turkey; [c]Mechanical Engineering Department, Middle East Technical University, Ankara, Turkey

ABSTRACT

In the current study, effects of two different underhood geometry modifications namely; fan position relative to shroud and fan tip clearance, on airflow through an agricultural tractor engine cooling system are investigated by utilizing CFD modeling. For the characterization of each modification, the underhood components are reduced to a domain of cooling systems including only fan, shroud, and radiator that allows saving in computational time and cost. The models are validated using a custom designed underhood flow setup, where hotwire velocity measurements at proximity to the radiator are conducted. The mass flow rate and the uniformity of the airflow through the radiator are quantified as performance parameters. For the former modification, position of fan relative to shroud, the computations are performed for the percentages of fan projection into shroud (FPiS) varying from 78% to 0% at fan rotational speeds of 2060 and 2800 rpm. The optimum fan location is found to be around 56–60% for both rotational speeds that leads 8% increase in mass flow rate compared with the pre-design location of 74%. In addition, a noticeable reduction in the relative magnitude of the RMS velocity through the radiator is obtained for the moderate FPiS values. For the latter modification, fan tip clearance, the computations are performed for the tip clearance values varying from 5.25to 12 mm at a fan rotational speed of 2060 rpm. As the tip clearance decreases up to 6 mm, air mass flow rate can be improved by 7%. However, further reduction in tip clearance does not improve the air mass flow rate instead it decreases, suggesting an optimum tip clearance value. The results suggest that the proper geometrical modifications in engine cooling systems might induce significant improvement in the aforementioned performance indicators.

ARTICLE HISTORY
Received 15 July 2018
Accepted 6 May 2019

KEYWORDS
CFD; underhood flow; engine cooling; optimization; fan; shroud

1. Introduction

In recent decades, increasing environmental considerations and desire for enhanced performances in the automotive industry have pushed the manufacturers to design high performance and downsized engines that fulfill the recent emission levels. Such designs generally result in increase in the heat flux and decrease in the airflow rate through the front end of the radiators. The geometrical constraints associated with the overall vehicle design affect the layout of the engine components in the underhood compartment. For heavy duty vehicles, the underhood cooling becomes more challenging issue compared to the passenger vehicles as a result of the operating conditions including, lack of ram air rate due to low vehicle speed, higher operating temperatures, payload capacity, and the dirty environment (Sofu et al., 2004). Proper modeling of aforementioned issues under the geometric constraints with proper assumptions appears as a challenging task for the analysis of underhood flow phenomena.

Along with the improvements in the modeling analysis techniques Computational Fluid Dynamics (CFD) tools have been widely used to model the real case application in a wide range spectrum including urban aerodynamics, nanofluid applications and internal combustion engine performance (Akbarian et al., 2018; Mou, He, Zhao, & Chau, 2017; Ramazanizadeh, Nazari, Ahmadi, & Chau, 2019). Considering the applications on underhood flow analysis, CFD tools can provide alternative, cost and time effective and powerful solutions during the preliminary design and the optimization of the design stages. In the early investigations of the numerical methods, one-dimensional approximation was commonly performed (Pang, Kalam, Masjuki, & Hazrat, 2012). In recent decades, advances in numerical techniques have made the computational fluid dynamic (CFD) tools powerful and cost effective alternatives on complex underhood airflows (Caltrider, Davis, Madhavan, & Veling, 1993; Costa, 2003; Dinc, Arslan, Akgun, & Almenar, 2010; Ding, Williams, Karanth, & Sovani, 2006; Pan, Schoon,

CONTACT Mehmet Metin Yavuz ymetin@metu.edu.tr

Putta, Ogale, & Chen, 2010) to figure out the impact of the simulations on design and development processes. Davis, Veling, Caltrider, and Madhavar (1993) performed three dimensional CFD simulations on the cooling system of light trucks; in addition they discussed the necessity for an underhood thermal management model. Sofu et al. (2004) employed three dimensional CFD simulations coupled with one-dimensional thermal-fluid model in order to assess cooling requirement of an off-road construction equipment using the experimental data. Tai, Cheng, and Liao (2007) performed practical and simplified modeling of vehicle front part based on finite volume methods. They were able to obtain a good agreement on velocity distributions with experimental data suggesting that the simplified configurations could be effectively used for front-end styling.

In recent decades cooling performance optimization in relation to the geometrical modifications, including underhood layout design and individual component modifications appears as a common methodology (Dangmali, Dhamangaonkar, & Atnurkar, 2013; Khaled, Harambat, & Peerhossaini, 2010; Lee & Hong, 2000; Manna & Kushwah, 2015; Shome, Kumar, Kumar, & Arora, 2006), however there still exist significant unresolved issues. Baskar and Rajaraman (2015) provided a review focusing on airflow management in automotive engine cooling systems. They discussed the role of the experimental and CFD techniques in detail and also summarized the factors affecting the cooling performance and overall vehicle aerodynamic drag. An early experimental study conducted by Taylor and Chu (1976) proposed the parameters affecting the performance of a truck cooling system that could be listed such that fan characteristics and fan projection into shroud (FPiS) are of highly significant parameters, while fan to radiator distance, radiator characteristics, and tip clearance are among significant parameters. They suggested the optimum fan projection into shroud value of 60–70% with indicating no significant contribution of shroud type on cooling performance. Hallqvist (2008) performed a parametric three-dimensional CFD study that investigates the various underhood installation parameters for heavy trucks. It was concluded that the depth of the fan into shroud and fan to radiator spacing are of critical parameters and the flow uniformity considerably affects the cooling capacity. Results of the study indicate that the highest flow rate through the radiator was achieved with 50% FPiS value, whereas the flow rate was found to be less with 67% FPiS value and the lowest with 33% FPiS value. Hu et al. (2011) conducted particle image velocimetry and pressure measurements to investigate the effect of the existence of the shroud and the depth of a truck fan into the shroud for various rotational speeds. They observed that the fan with shroud had higher exit velocities than fan without shroud and 60% FPiS value exhibited the highest performance in terms of flow rate and the pressure rise for all rotational speeds. Mehravaran and Zhang (2015) performed CFD simulations along with wind tunnels tests to quantify the effects of fan projection into shroud, different shroud geometries and tip clearance on the airflow through an automobile engine cooling system. It was concluded that decreasing the tip clearance resulted in improvement of airflow, and an interval of 60–70% FPiS value demonstrated better performances for most of the shrouds they studied. Venter and Kröger (1992) proposed a method to present the effect of tip clearance on the performance of an axial flow fan showing that decreasing tip clearance results in improvement of performance of the axial fan.

The current study aims to investigate the effects of two different underhood geometry modifications, fan position relative to shroud and fan tip clearance, on airflow through the engine cooling system of a newly designed agricultural tractor, using computational fluid dynamics (CFD) modeling. For this purpose, the solution domain is simplified to cooling package components including fan, shroud, and radiator. The flow is assumed to be incompressible and adiabatic (no heat transfer effect). For the relative fan position cases, the simulations are performed at rotational speeds of 2060 and 2800 rpm for FPiS values varying from 78% to 0%. For tip clearance cases, the simulations are performed for the tip clearance values varying from 5.25–12 mm at a fan rotational speed of 2060 rpm.

2. Model development

The CFD model was constructed over three-dimensional full-scale geometry using ANSYS SpaceClaim. ANSYS Meshing was used for mesh generation and ANSYS FLUENT was utilized in order to perform the flow simulations. The model geometry was reduced to cooling package components of Turk Traktör's one of the specialty type agricultural tractor including; fan, shroud, and radiator. The system components (fan, shroud, and radiator) and the corresponding fluid domains (MRF and radiator core) are shown in Figure 1(a). The cooling package was centered in a rectangular prism domain with dimensions of 2 m wide, 2 m deep and 6 m long, which is shown in Figure 1(b). The fan model has 10 blades with overall diameter, hub diameter, and hub thickness values of 480, 189 and 57.5 mm, respectively. The details of the simulation geometry are provided in Table 1.

Considering the study for the position of fan relative to shroud, to be consistent with the literature (Hallqvist, 2008) the depth of the fan into the shroud was quantified

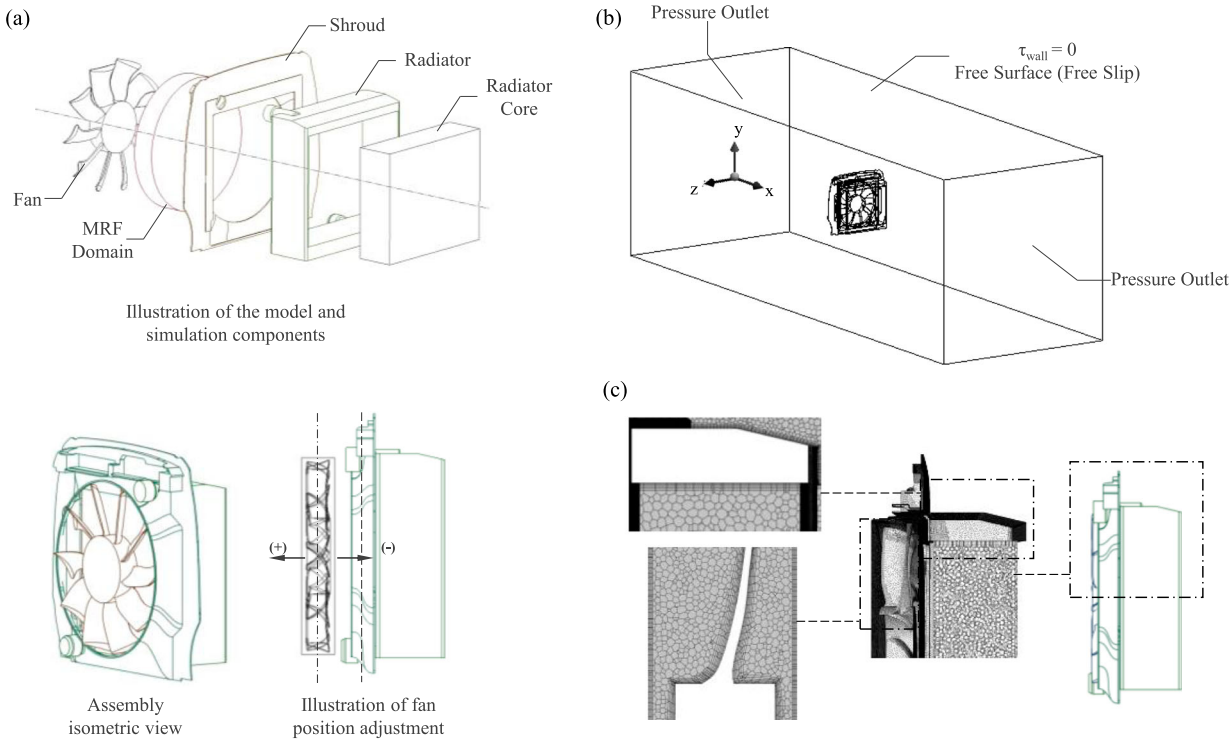

Figure 1. (a) Illustration of CFD model; components, assembly view and fan position adjustment, (b) typical simulation domain and boundary conditions used in CFD model, (c) slices of the mesh on fan blades-MRF domain and radiator core.

Table 1. The details of the simulation geometry.

Parameter	Specification
Total Enclosure Width	2 m
Total Enclosure Depth	2 m
Total Enclosure Length	6 m
Fan Diameter	480 mm
Fan Hub Diameter / Hub Thickness	189 mm / 57.5 mm
No. of Fan Blades	10
Radiator Core Thickness	140 mm
Radiator Core Frontal Area	0.2 m^2

using the percentage FPiS, which was calculated by taking the ratio of the fan volume occupied in the shroud to entire fan volume. For that purpose, the outer circular surface of the shroud and the inward surface of the fan hub were taken as reference. The pre-design configuration of the cooling package had 74% fan projection into the shroud corresponding to 42.6 mm depth of the fan thickness. The fan geometry was translated along the x-axis both in 'positive' and 'negative' directions as illustrated at the bottom part of Figure 1(a). Different FPiS values were tested varying from 78% to 0% leading to 2 and 43 mm maximum translations from the pre-design configuration in positive and negative directions, respectively.

In order to quantify the effect of tip clearance on underhood flow, four additional shrouds with tip clearance values of 5.25, 8, 10 and 12 mm were modeled and compared with the base case, which was the pre-design condition and had a tip clearance value of 6 mm.

Hallqvist (2008) summarizes that, the performance of the cooling systems strongly depends on the amount of the mass flow rate along with the considerations of the velocity and the temperature distributions. Since the ultimate aim of the current study is to investigate the influence of the geometrical modifications on the underhood airflow, the performance estimations are based on the mass flow rate through the radiator, velocity distribution and its uniformity on the radiator. This approach is also in line with similar studies conducted in the literature (Hallqvist, 2008; Mehravaran & Zhang, 2015). The uniformity is tried to be quantified by root mean square (RMS) of the velocity distribution of radiator surface which is calculated via Equation (1):

$$V_{\mathrm{RMS}} = \sqrt{\frac{\sum_{i=1}^{N} (V_i - V_{\mathrm{ave}})^2}{N-1}} \tag{1}$$

where N is number of nodes, V_i is the velocity of each node, V_{ave} is average velocity across the surface of interest. The aforementioned parameters are selected because they represent the underhood airflow quantitatively and qualitatively, which is quite deterministic on heat removal from the radiator therefore the overall cooling performance of the engine compartment.

Table 2. Boundary conditions and simulation matrix.

Parameter	Specification
Air Density	1.127 kg/m^3
Turbulence Model	Realizable k-ϵ
Top, Bottom, and Side Walls	Free Slip
Inlet	Pressure
Outlet	Pressure
Components' (shroud, fan blades, radiator) wall surfaces	No Slip
Radiator Core	Porous Medium
Fan Model	MRF
Fan Speeds	2060, 2800 rpm
FPiS (Fan Projection into Shroud) Range	0–78%
Tip Clearance Range	5.25–12 mm

Table 3. Mesh parameters used in the mesh independence study.

Algorithm	Polyhedral elements		
Method	Patch conforming		
	Mesh 1	Mesh 2	Mesh 3
Nodes	5,602,975	9,290,237	18,392,721
Elements	2,574,797	3,570,809	5,702,415

The top, bottom and side surfaces of the domain were specified as free slip boundary condition where the flow was free to move without any resistance. At the inlet and the outlet of the computational domain the pressure boundary condition was imposed to simulate the atmospheric condition. The wall surfaces of cooling package components including shroud, fan blades and radiator were modeled as no slip boundary condition where the fluid had zero velocity relative to adjacent walls. The details of the boundary conditions along with the simulation matrix are provided in the Table 2.

In order to capture the complex airflow and to obtain a robust solution, the fan was modeled as Multiple Reference Frame (MRF) methodology. The fan geometry was centered in the MRF domain of 490 mm diameter and 80 mm thickness. Two different rotational speeds 2060 and 2800 rpm were tested to simulate the operating conditions namely; moderate duty and high duty operations. The radiator was modeled as fluid domain with porous medium, which restricted the fluid to flow in one direction. Experimental air velocity (m/s) versus pressure drop (Pa) of the radiator data, provided by the manufacturer, was used to determine the pressure drop characteristics of the heat exchangers using the following function below;

$$\Delta p = Au_i + Bu_i^2 \tag{2}$$

where u_i was the superficial velocity through the medium, and A and B were the polynomial constants to calculate inertial resistance and viscous resistance coefficients in the porous model, respectively. ANSYS Fluent uses Equation (3) to simulate a porous medium,

$$\left(\frac{\partial p}{\partial x}\right)_{\text{porous}} = \left[D_i \mu u_i + \frac{1}{2} F_i \rho u_i^2\right] \Delta L \tag{3}$$

where D_i and F_i are the inertial resistance and viscous resistance values, respectively. μ and ρ are dynamic viscosity and density at the test conditions, whereas ΔL is the thickness of the porous medium in the model. The simulations in the present study were conducted with dummy inertial and viscous resistance values different from the calculated ones using Equations (2) and (3) due to the confidentiality issues in revealing the results of the actual cooling system. Resistances in other directions are taken at least two orders of magnitude higher than the obtained resistances for the flow direction to restrict the flow to one direction.

For the grid generation, the unstructured mesh consisting three-dimensional polyhedral elements and prismatic inflation layers were constructed. Patch conforming methodology was utilized for the mesh creation. The total thickness of the boundary layer was calculated for each particular surface such as fan blades, shroud, side surface of the MRF domain, and side walls of the radiator core using the turbulent flow over boundary layer equations considering the expected Reynolds numbers over these surfaces. Utilizing these total thickness values, number of the total inflation cells were defined for each surface in order to resolve the boundary layer flows adequately. First layer thicknesses of the inflation layers were also set to values that were expected to keep the total number of mesh cells in a reasonable size and provide y+ values that were suitable to work with near wall treatment solver. The sample images of the mesh generated for the upper half of the cooling package and the fan blades embedded in MRF along the symmetry plane are shown in Figure 1(c). The flow through the underhood compartment is highly turbulent and unsteady. In order to investigate the significant flow characteristics, a suitable turbulence model should be selected. Considering the similar CFD modeling studies reported in literature, the standard and realizable $k-\varepsilon$ turbulence models were shown good agreement with experimental data (Katoh, Ogawa, & Kuriyama, 1991; Mehravaran & Zhang, 2015; Soe & Khaing, 2017; Venter & Kröger, 1992; Yang, Wang, Dang, & Li, 2015). Therefore, in the current study, the realizable $k-\varepsilon$ turbulence model was utilized along with the enhanced wall treatment considering that it addresses the deficiencies of the standard and RNG k-ϵ models as explained by Soe & Khaing, 2017. For the discretization scheme, both first order and second order upwind schemes were considered for spatial discretization of the momentum, turbulent kinetic energy and turbulent dissipation rate. For two sample cases, the simulations were

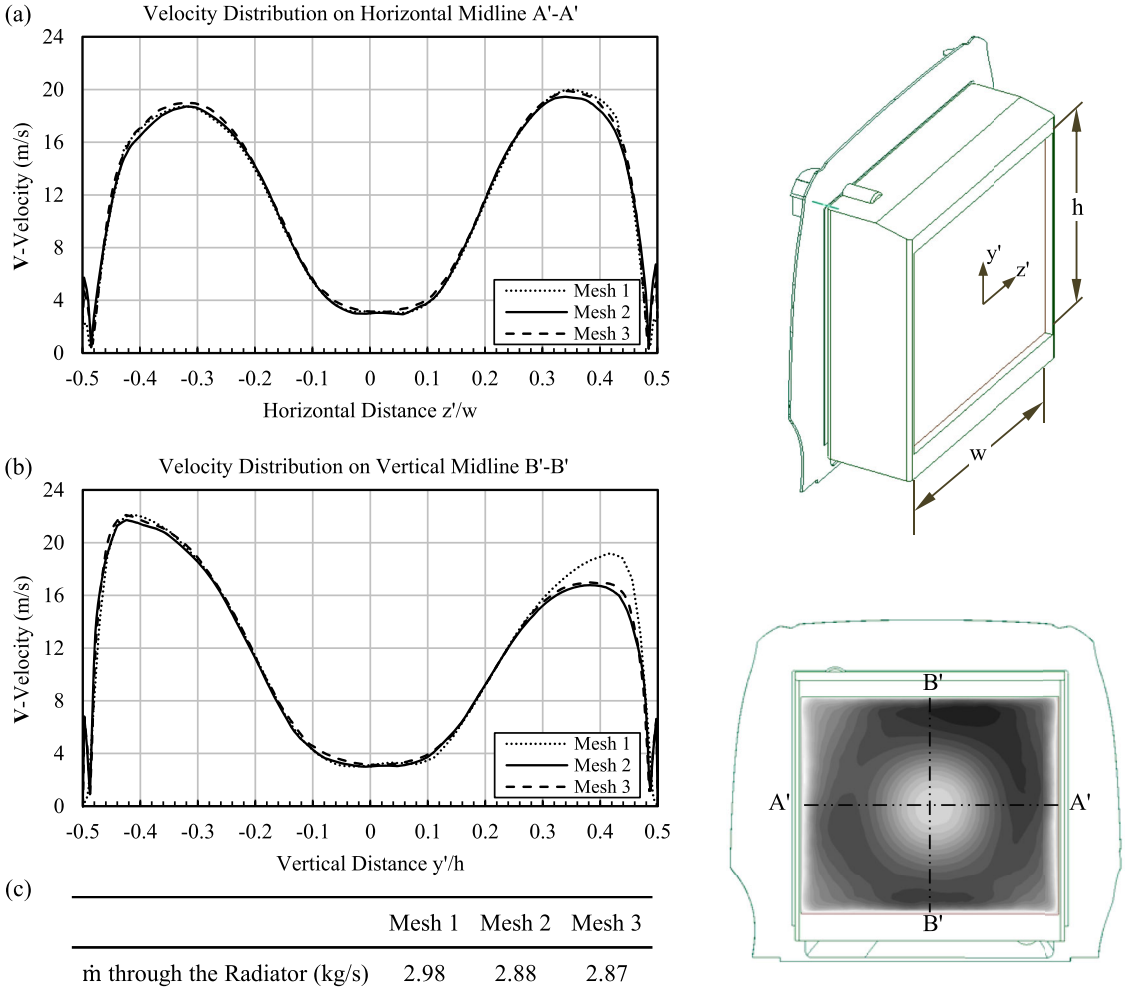

(c)

	Mesh 1	Mesh 2	Mesh 3
$\dot{m}$ through the Radiator (kg/s)	2.98	2.88	2.87

Figure 2. Velocity distribution along the horizontal and vertical midlines on radiator inlet surface for three different meshes.

conducted for both schemes and the differences in the solutions were reported both qualitatively and quantitatively. The general flow patterns were quite similar except at regions far downstream of the fan and thus away from the region of interest. Considering the velocity magnitudes at the regions upstream of the fan, the maximum of 10% variations were observed at some isolated points where for the majority of the domain ($\sim$90%) the variations in the velocity magnitudes were even less than 1%. More importantly, when the mass flow rates through the radiator were considered, it was observed that the deviation was less than 0.1% with switching the discretization scheme from second order to first order. Considering the deviations obtained in the sample cases along with the fact that the convergence was more robust and easily obtained at significantly shorter time with the first order discretization scheme, the rest of the simulations were conducted using the first order discretization scheme. The COUPLED scheme which is based on a pressure based algorithm was preferred as the pressure velocity coupling scheme. This scheme is known to be a robust and efficient single phase implementation for steady state analysis.

A typical simulation of the entire domain accounts for six hours of computational time. The convergence behavior of the simulation was monitored by plotting the residual values of the velocity components on the several points located near the fan and the radiator core. In addition, the sum of the normalized residuals for mass conservation and momentum conservation equations were taken into account.

The flow simulations were calculated by solving the following steady state, incompressible form of the mass and momentum conservation equations.

$$\frac{\partial u_i}{\partial x_i} = 0 \tag{4}$$

$$u_j \frac{\partial u_i}{\partial x_j} = -\frac{1}{\rho}\frac{\partial p}{\partial x_i} + \nu \frac{\partial^2 u_i}{\partial {x_j}^2} \tag{5}$$

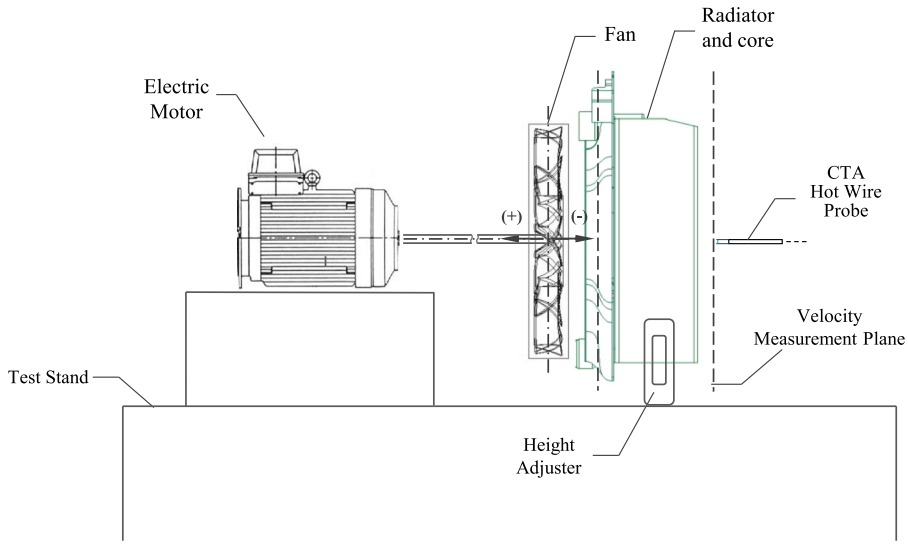

Figure 3. Illustration of the experimental test bench.

Table 4. The dimensions of the radiator, fan and CFD model enclosure for the validation study.

Parameter	Specification
Total Enclosure Width	4 m
Total Enclosure Depth	2.8 m
Total Enclosure Length	4.5 m
Fan Diameter	414 mm
Fan Hub Diameter / Hub Thickness	189 mm / 57.5 mm
No. of Fan Blades	10
Radiator Core Thickness	85 mm
Radiator Core Frontal Area	0.163 m^2

In these Equations (4) and (5) ρ, u, p and ν stand for density, velocity, pressure and kinematic viscosity respectively. The turbulence properties of the simulation were accounted by utilizing realizable $k-\varepsilon$ turbulence model along with the enhanced wall treatment function that solves the following transport equations for turbulent kinetic energy k and energy dissipation rate ε.

$$\frac{\partial}{\partial x_j}(ku_j) = \frac{\partial}{\partial x_j}\left[\left(\nu + \frac{\nu_t}{\sigma_k}\right)\frac{\partial k}{\partial x_j}\right] + \nu_t S^2 - \varepsilon \tag{6}$$

$$\frac{\partial}{\partial x_j}(\varepsilon u_j) = \frac{\partial}{\partial x_j}\left[\left(\nu + \frac{\nu_t}{\sigma_\varepsilon}\right)\frac{\partial \varepsilon}{\partial x_j}\right] + C_1 S\varepsilon - C_2\frac{\varepsilon^2}{k+\sqrt{\nu\varepsilon}} \tag{7}$$

In the above Equations (6) and (7) ν_t represents the eddy viscosity. σ_k and σ_ε are the turbulent Prandtl numbers for k and ε, respectively. S is the modulus of the mean rate-of-strain tensor, defined as$S = \sqrt{2S_{ij}S_{ij}}$ where $S_{ij} = (1/2)((\partial u_i/\partial x_j) + (\partial u_j/\partial x_i))$. $C_1 = \max[0.43, (\eta/\eta+5)]$, where $\eta = (Sk/\varepsilon)$. $C_2 = 1.9$.

In order to ensure that the solutions were independent from the mesh intensity, the mesh independence study was performed utilizing the grid refinement for the cooling package configuration without any modification. The details of the meshes used in the mesh independence study are presented in Table 3. Three different mesh topologies were constructed from coarsest to finest structure namely mesh 1, mesh 2, and mesh 3, respectively. The coarsest mesh 1 had 5,602,975 nodes whereas fine mesh 2 and the finest mesh 3 had 9,290,237 nodes and 18,392,721 nodes, respectively. In order to provide a comprehensive comparison, Figure 2 is constructed for the velocity magnitude V along the horizontal and vertical midlines on the radiator front surface. The sketches of the midlines along with the local coordinates (y', z') on the geometry are also illustrated in Figure 2. Figure 2(a) shows the velocity magnitude V along the horizontal midline A-A whereas Figure 2(b) shows velocity magnitude V along the vertical midline B-B. It can be seen that the velocity magnitudes on the radiator front surface are not axisymmetric due to the fact that the shroud design is not fully symmetric as demonstrated in Figure 1(a). The velocity distribution along the vertical midplane of radiator front surface clearly shows the mesh size dependency while it does not exhibit any considerable change along horizontal midplane. The results indicate that velocity values differ a maximum of 18% between meshes 1 and 3. However, the velocity magnitudes vary a maximum of 2% between meshes 2 and 3 for both midlines. In addition, the mass flow rate values through the radiator inlet are also tabulated in Figure 2(c), which are also in line with the aforementioned results. Mass flow rate differs up to 4% between meshes 1 and 3 while it differs less than 0.5% between meshes 2 and 3. Considering all these results, mesh 2 was chosen as mesh independent case and used for further analyses.

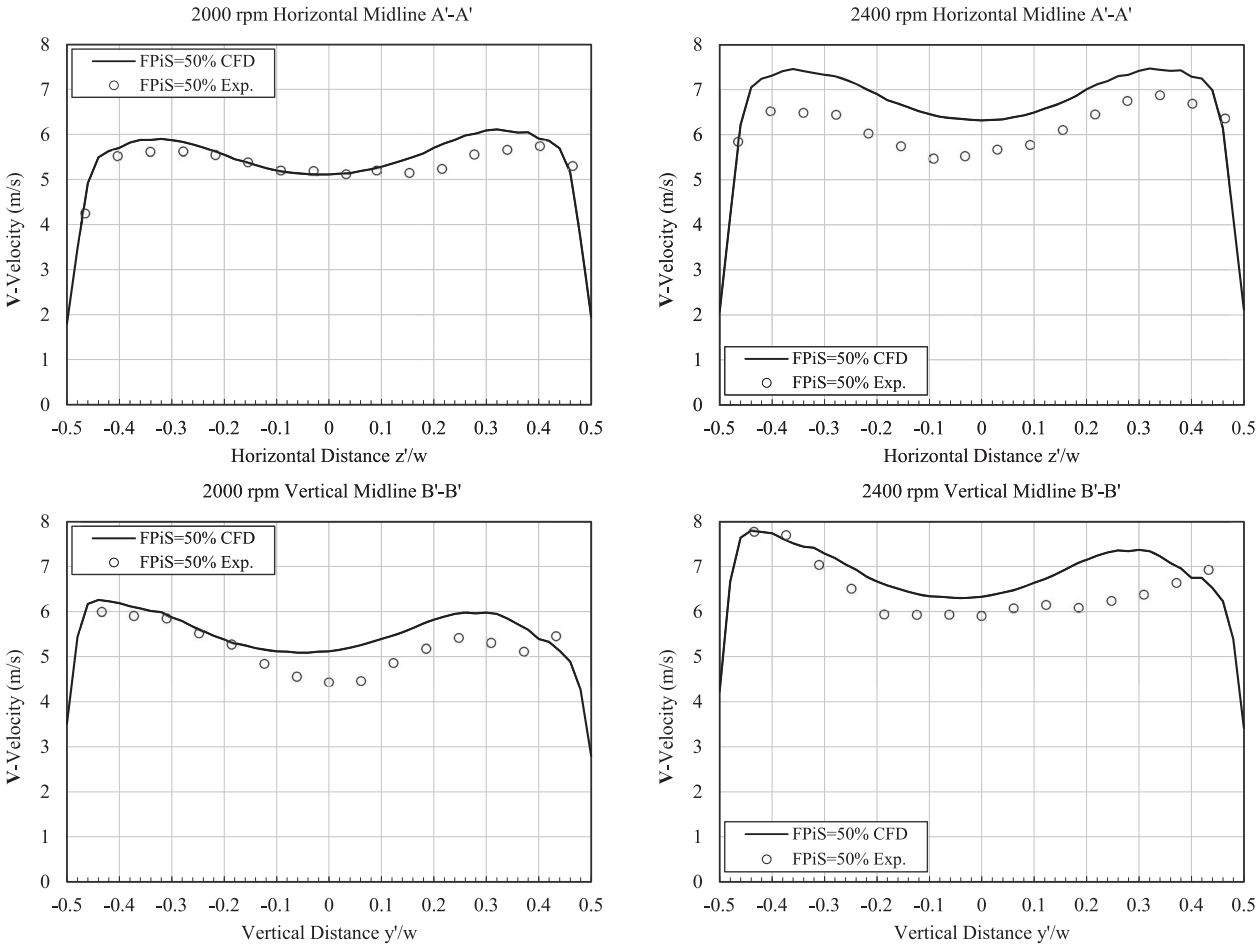

Figure 4. The velocity distributions along the horizontal and vertical midlines on a plane 23 mm upstream of the radiator for the validation study.

2.1. Validation study

The underhood air flow test bench was built to quantify the velocity in the cooling package, where the velocity information was used for validation purpose in the present study. The sketch of the set up is illustrated in Figure 3. The system allows positioning of various components of the cooling package. The fan speed is adjusted using a PLC controlled electrical motor. A computer controlled traverse mechanism is used to position the constant temperature hot-wire anemometry probe in three dimensions with high accuracy. The validation study was conducted with a cooling package already available including a commercial radiator and its' shroud coupled with a cooling fan, where the corresponding CFD models were also developed. The experiments were performed for two different fan speeds 2000 and 2400 rpm for 50% fan projection into the shroud. The air velocity distribution upstream of the radiator core was measured using a Dantec hot-wire probe, which was positioned on

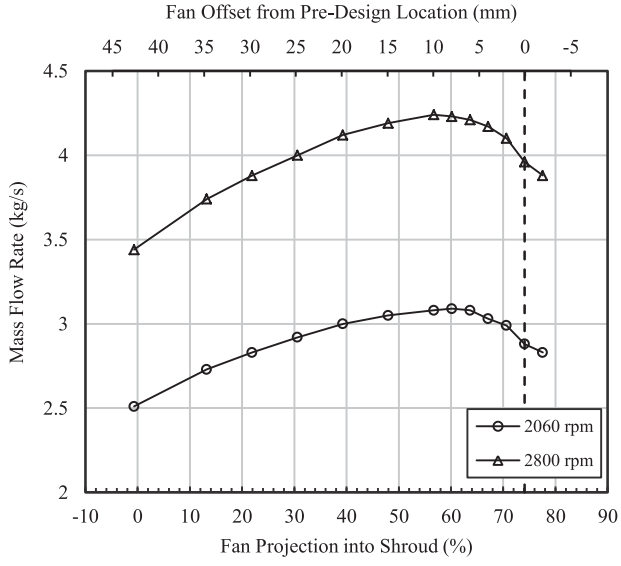

Figure 5. Variation of mass flow rate through the radiator with varying fan position relative to shroud.

a measurement plane at 23 mm upstream of the radiator core. The probe was traversed horizontally and vertically to acquire the velocity distributions on the midlines previously introduced in Figure 2. The measurement points were selected 25 mm apart and the relative uncertainty of the velocity measurements was calculated as 4%.

For the validation study, the CFD model has been developed to closely represent the test bench case for which the dimensions of the radiator and CFD model enclosure are given in Table 4. Solver settings, turbulence model, and boundary conditions are kept same as tabulated in Table 1. The results obtained from the experimental and the numerical studies are plotted in Figure 4 such that graphs on the left column represent the results of 2000 rpm fan speed for horizontal and vertical midlines, respectively, whereas the graphs on the right column represent the results of 2400 rpm fan speed. The velocity plots are constructed using the same approach explained for Figure 2.

Considering the plots for 2000 rpm fan speed, the test and CFD results agree well particularly on the horizontal midline, where the deviation between experimental and numerical results varies from minimum of 0.1% to maximum of 10.5%, where the average value is calculated as 4.4%. On the vertical midline, this deviation varies from 0.7 to 17.2%, and is 8.1% in average. Overall, the trends of velocity distributions indicate quite similar behaviors. For the fan speed of 2400 rpm, the deviation between experimental and numerical results vary from 0.2–17.7%, whereas the average values on the horizontal and vertical midlines are 11.5% and 7.9%, respectively. Although the similar velocity trend lines are successfully achieved via CFD analyses, the amount differences in obtained velocities are believed to be related to simplified 3D solid geometries in CFD analysis, uncertainty in velocity measurements, the effect of directionality in velocity on hot wire anemometry, and porosity settings of the radiator.

3. Results and discussions

3.1. Effect of fan position relative to shroud on underhood airflow

Variation of the mass flow rate through the radiator with varying the fan position relative to the shroud is shown in Figure 5 for both fan speeds of 2060 and 2800 rpm. The lower horizontal axis represents the percentage fan projection into shroud while the corresponding movement of the fan in mm scale from its pre-design location of 74% FPiS is represented in the upper horizontal axis. The dashed line indicating the initial location is added to the graph in order to identify the relative fan position clearly. MRF model is used to simulate the fan, which encloses a volume around the fan. The maximum attainable percentage fan projection into shroud without having a contact on the surfaces of the MRF volume and the radiator core is 78%. Therefore, variation of the fan position in the figure is limited to 0% and 78%, which represents the cases of no projection into the shroud and maximum possible projection into the shroud in the simulation model, respectively. One can easily infer from the figure that decrease in FPiS from the maximum value of 78% up to 56% results in increase in mass flow rate for both rotational speeds, where up to 8% increase in mass flow rate is achieved around 56%–60% FPiS compared to the pre-design FPIS of the fan. Further decrease in FPiS from 56% to 0% yields continuous decrease in mass flow rates. It can also be inferred from the figure that giving a 26 mm offset to the fan results in the same mass flow rate that can be reached when the fan is located at its initial position. Even though the obtained results are believed to be dependent on the specific designs of fan and shroud that are used in the simulation model, they are quite in line and show a similar trend with the observations of the similar studies in the literature (Hallqvist, 2008; Hu et al., 2011; Mehravaran & Zhang, 2015; Taylor & Chu, 1976) for different cooling packages, in which the highest flow rates are achieved between the FPiS values of 60% and 70%.

The horizontal and vertical midlines that were previously introduced in Figure 2, are used to demonstrate the velocity distribution along the radiator inlet surface in Figure 6 for fan position relative to shroud values varying from 0% to 74% at fan rotation speeds of 2060 rpm (charts on the left) and 2800 rpm (charts on the right). Considering the overall distributions in the charts, higher velocity values appear at the regions corresponding to the fan blades, whereas lower velocity distributions are seen around fan hub region for both fan rotation speeds as expected. In addition, at regions close to the blade tips and shroud there exist strong velocity gradients which can be attributed to wall boundary layer and porosity interaction with radiator and its core.

For FPiS values varying between 74% and 48%, there exist higher velocity peaks at the proximity of fan blades in both axes. This observation suggests that the effect of improvement in mass flow rate for 60% and 48% is evident in velocity distribution as expected. In addition, 74% fan projection exhibits the lowest velocity values around the hub region in all charts since it causes the earlier stagnation in main flow direction. Any decrease in FPiS value leads increase in velocity magnitude around the hub region. It should also be pointed that the deviation between the highest and the lowest velocity regions is

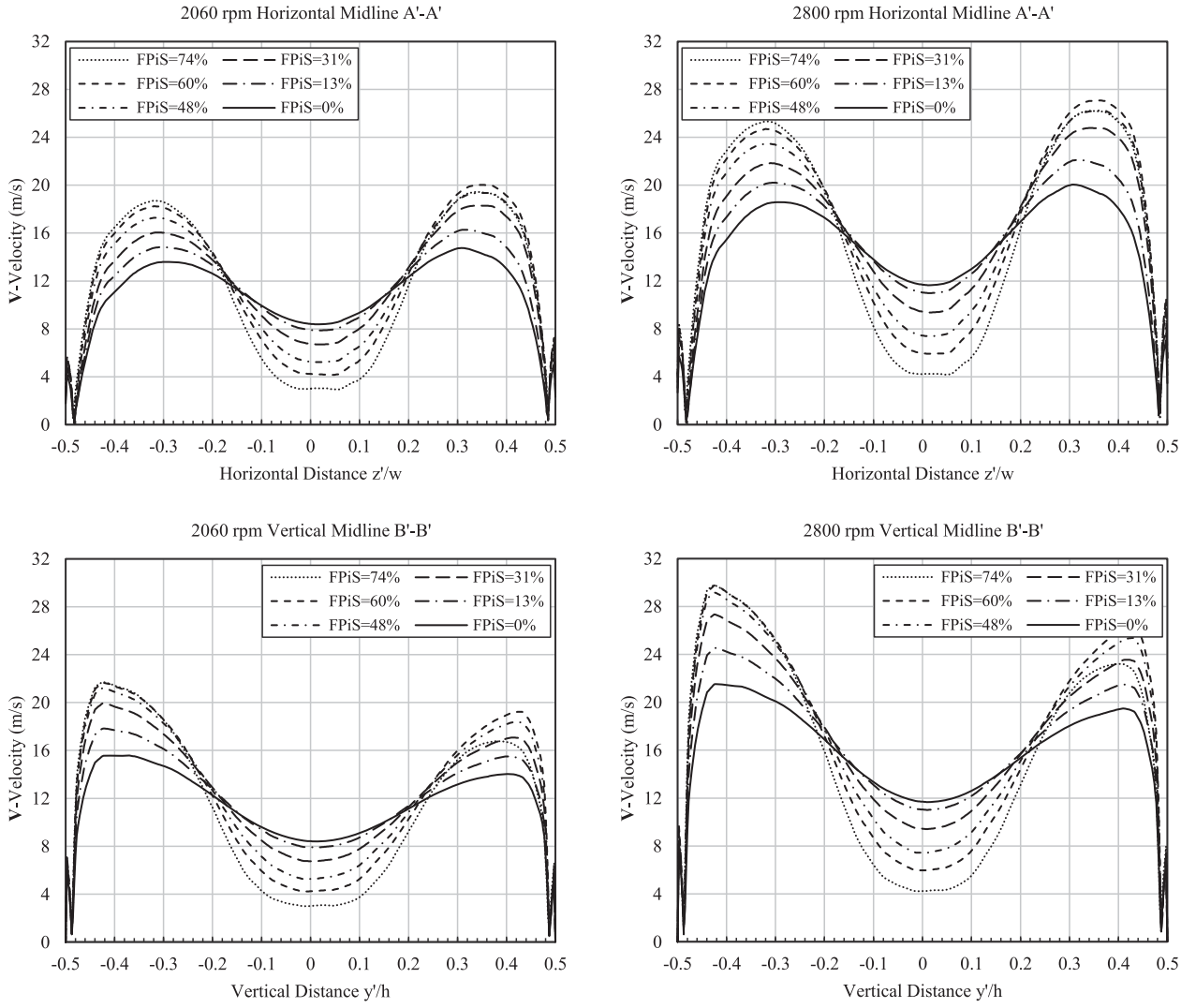

Figure 6. Velocity distribution along the horizontal and vertical midlines on radiator inlet surface for varying fan position relative to shroud.

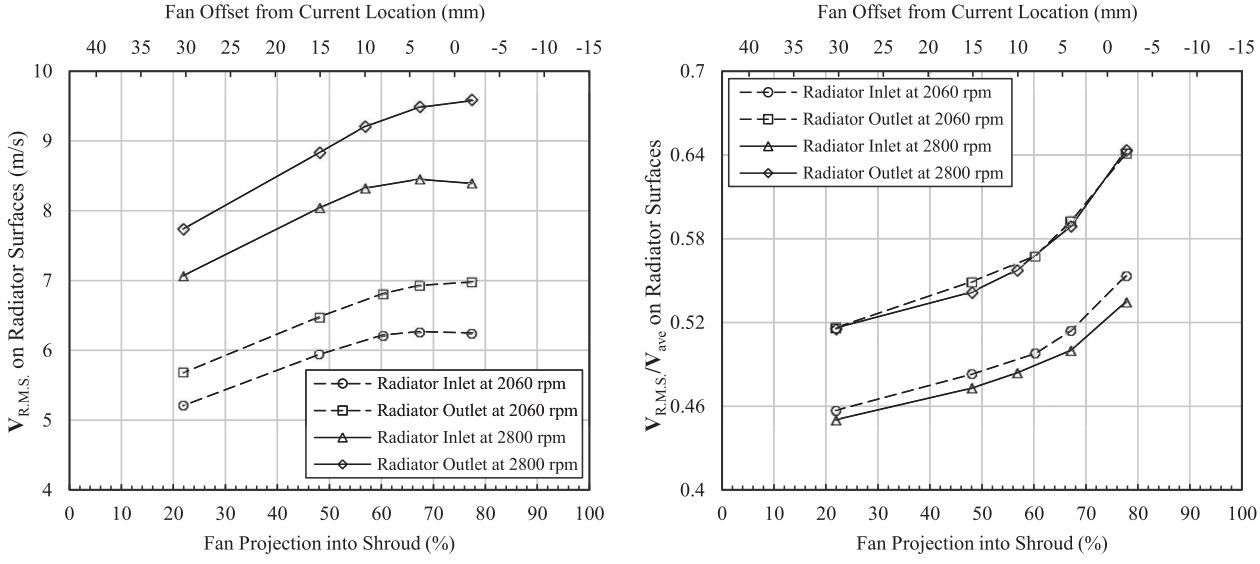

Figure 7. Effect of fan position relative to shroud on uniformity of velocity distribution on radiator inlet and outlet surfaces.

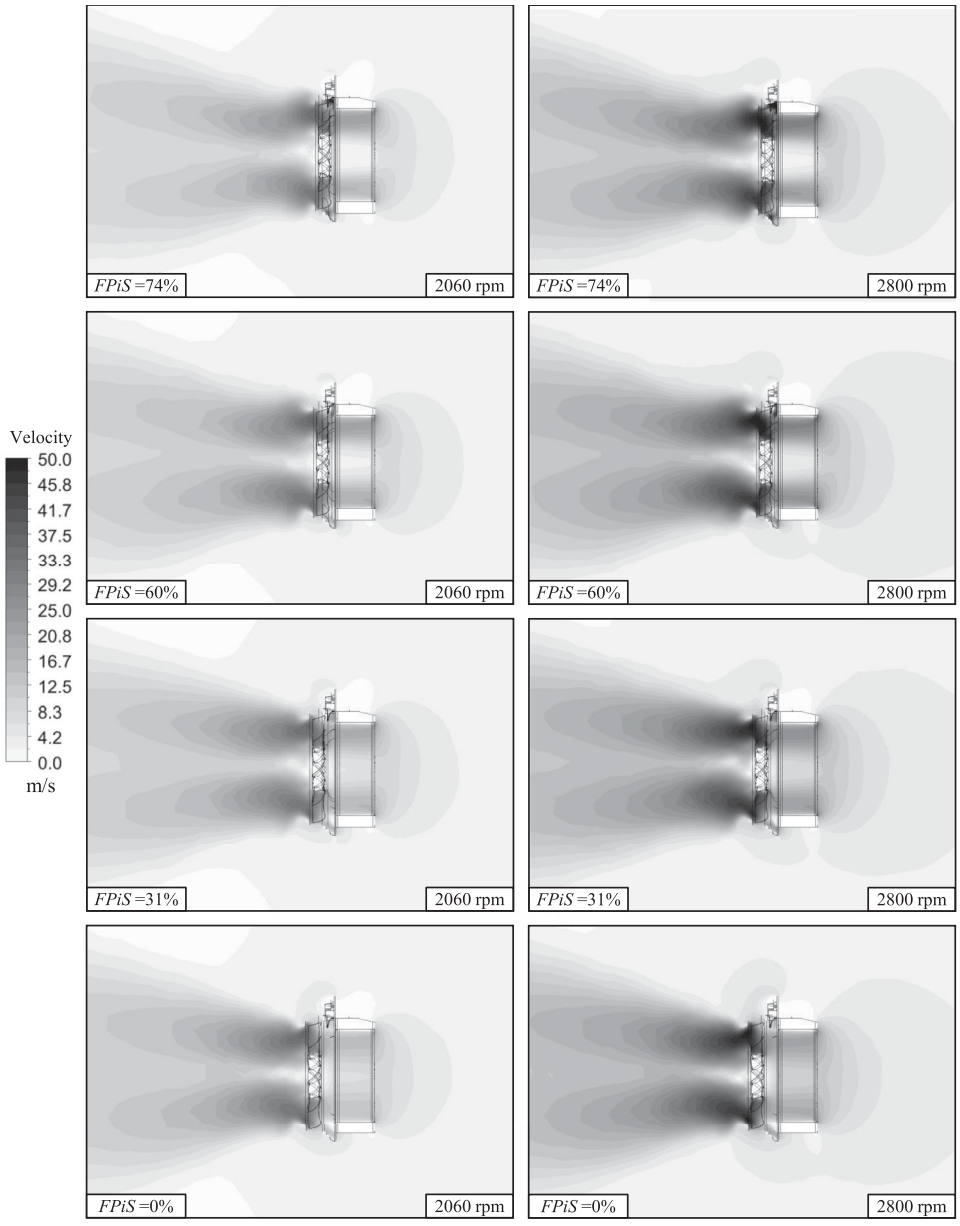

Figure 8. Velocity contours at mid-section plane along x-axis for FPiS values 74%, 60%, 31% and 0% at fan speeds of 2060 and 2800 rpm.

relatively larger for the FPiS values varying between 48% and 74% whereas there exist smaller deviation for lower FPiS values at both horizontal and vertical axes.

To quantify the aforementioned concept of non-uniformity of velocity distribution on radiator surfaces, root mean square of velocity (V_{RMS}) and its non-dimensional representation, which is normalized by the average velocity on the radiator surface (V_{RMS}/V_{ave}), are demonstrated in the left and the right charts of Figure 7, respectively. The upper and lower horizontal axes of both charts are indicated by the scales used in Figure 5. Considering the results of velocity RMS presented in the left chart, there are significant increases in RMS values of the velocities on both inlet and outlet surfaces of the radiator as the FPiS value increases, which is the indication of fan getting closer to the radiator. In addition, the results indicate that the radiator outlet surface possesses higher RMS values compared to the radiator inlet surface. Considering the V_{RMS}/V_{ave} values, which can be named as relative non-uniformity and demonstrated in the right chart of Figure 7, it is observed that even though the general trends of the charts are consistent with the trends seen in velocity RMS graphs, there are two major differences, which become apparent due to normalization. Firstly, at both fan speeds the V_{RMS}/V_{ave} curves exhibit similar trend indicating that the relative non-uniformity is independent from the fan speed on both radiator surfaces. Secondly, the slopes of the V_{RMS}/V_{ave} curves become

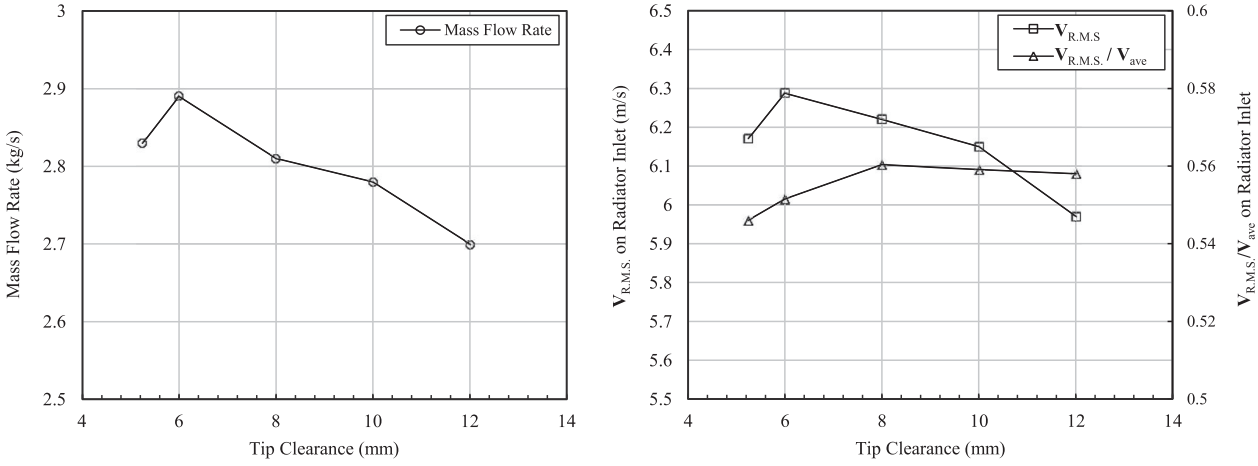

Figure 9. Variation of mass flow rate through the radiator core and uniformity of velocity distribution on inlet surface with varying fan tip clearance at fan speed of 2060 rpm.

sharper with increasing FPiS values. It should also be noted that the optimum mass flow rate location of 60% FPiS yields a considerable reduction in V_{RMS}/V_{ave}, relative non-uniformity, in the order of 10% while providing an 8% increase in mass flow rate compared to the pre-design condition.

In order to further investigate the effect of the fan projection on overall flow structure of underhood, constant contours of velocity magnitude along the x-axis at mid-section plane are shown in Figure 8. Figure 8 is constructed such that left column represents the velocity contours for fan speed of 2060rpm and right column represents the fan speed of 2800 rpm for selected FPiS values of 74%, 60%, 31% and 0% from top to bottom, respectively. Velocity contours of the radiator core indicate that less air flow occurs at the projection of the fan hub on the radiator core at high FPiS values, whereas the flow becomes more uniform throughout the radiator core by increasing the distance between the fan and the radiator. One can also infer from the velocity contours that the overall flow field shows similar flow patterns for both fan rotational speeds where a suction region occurs prior to the radiator inlet along with a strong discharge region at the fan exit due to the accelerated air flow by the fan.

3.2. *Effect of fan tip clearance on underhood airflow*

Variation of the mass flow rate through the radiator core and the uniformity of velocity distribution on radiator inlet surface in terms of V_{RMS} and V_{RMS}/V_{ave} at the fan rotational speed of 2060rpm are shown in left and right charts of Figure 9, respectively for fan tip clearance values of 5.25 mm, 8 mm, 10 mm and 12 mm as well as the pre-design tip clearance value of 6 mm. The trend in the left chart indicates that increasing the tip clearance yields decrease in the mass flow rate up to 7% with respect to pre-design tip clearance value due to having more leakage through the clearance region. Decreasing the tip clearance value less than 6 mm also reduces the mass flow rate by 2%, which is believed to be due to the interaction between the flow and the boundary layer on the shroud wall. Considering the non-uniformity distributions shown in the right chart of Figure 9, RMS of the velocity decreases with either increasing or decreasing the tip clearance from the pre-design value of 6 mm. At tip clearance values of 12 mm and 5.25 mm, V_{RMS} decreases by 5% and 2%, respectively, with respect to the tip clearance value of 6 mm. For the relative non-uniformity where RMS velocity is normalized with average velocity, V_{RMS}/V_{ave}, a trend of decreasing positive slope with a peak value at 8 mm tip clearance is observed.

4. Conclusion

In the current study, the effects of two different underhood geometry modifications including fan position relative to shroud and fan tip clearance, on airflow of an agricultural tractor engine cooling system are studied using CFD modeling. The results of CFD models are confirmed with the velocity measurements in a custom designed underhood flow setup. It is shown that RMS calculation for spatial domain to evaluate the non-uniformity of the flow through the radiator can be used as a performance indicator. The results show that for both rotational fan speeds of 2060 and 2800 rpm, the optimum FPiS value is in the range of 56%–60%, which yields a considerable reduction in V_{RMS}/V_{ave}, relative non-uniformity, while providing an 8% increase in mass

flow rate compared to the pre-design fan – shroud orientation. Moreover, performed calculations for various tip clearance distances reveal that this parameter also has a significant role in mass flow rates. Decreasing the tip clearance from 12 mm to 6 mm yields 7% increase in mass flow rate due to reduction in the leakages, however, further decrease in tip clearance does not improve the air mass flow rate, instead it decreases due to boundary layer interactions, which suggests an optimum tip clearance value. To sum up, the optimum orientation for the studied cooling package is determined via consecutive CFD iterations, in which the results indicate that 56%–60% FPiS value along with 6 mm tip clearance is the best condition among the simulated cases considering the highest flow rate through the radiator with minimum relative non uniformity, which are believed to be quite critical for the cooling performance of the radiator.

Acknowledgements

The authors would like to thank Prof. Dr. Mustafa İlhan Gökler from METU Biltir Center and OTEST Inc, for providing the working environment in METU Technopolis. The fruitful contributions of Dr. Hakan Mencek and Atayıl Koyuncu from TürkTraktör R&D are also gratefully acknowledged.

Disclosure statement

No potential conflict of interest was reported by the authors.

Funding

This work, which was primarily supported by the Scientific and Technological Research Council of Turkey (TÜBİTAK) [grant number 3151082], was produced with TürkTraktör and OTEST Inc.

ORCID

İlhan Öztürk http://orcid.org/0000-0002-7557-9892

References

Akbarian, E., Najafi, B., Jafari, M., Faizollahzadeh Ardabili, S., Shamshirband, S., & Chau, K. W. (2018). Experimental and computational fluid dynamics-based numerical simulation of using natural gas in a dual-fueled diesel engine. *Engineering Applications of Computational Fluid Mechanics*, *12*(1), 517–534. doi:10.1080/19942060.2018.1472670

Baskar, S., & Rajaraman, R. (2015). Airflow management in automotive engine cooling system – overview. *International Journal of Thermal Technologies*, *5*(1), 1–8.

Caltrider, J. L., Davis, F. V., Madhavan, R., & Veling, T. R. (1993). *Impact of computer aided engineering on ford light truck cooling design and development processes* (No. 931104). SAE Technical Paper. doi:10.4271/931104

Costa, E. A. (2003). *CFD approach on underhood thermal management of passenger cars and trucks* (No. 2003-01-3577). SAE Technical Paper. doi:10.4271/2003-01-3577

Dangmali, V., Dhamangaonkar, P. R., & Atnurkar, A. (2013). *CFD simulation of under hood engine compartment for forklift truck* (No. 2013-01-2861). SAE Technical Paper. doi:10.4271/2013-01-2861

Davis, F. V., Veling, T. R., Caltrider, J. L., & Madhavar, R. (1993). *Impact of computer aided engineering on Ford Motor Company light truck cooling design and development processes* (No. 932977). SAE Technical Paper. doi:10.4271/932977

Dinc, C., Arslan, O., Akgun, T., & Almenar, R. (2010). *Improvement of engine cooling performance for a construction truck using numerical and experimental methods* (No. 2010-01-2054). SAE Technical Paper. doi:10.4271/2010-01-2054

Ding, W., Williams, J., Karanth, D., & Sovani, S. (2006). *CFD application in automotive front-end design* (No. 2006-01-0337). SAE Technical Paper. doi:10.4271/2006-01-0337

Hallqvist, T. (2008). *The cooling airflow of heavy trucks – a parametric study* (No. 2008-01-1171). SAE Technical Paper. doi:10.4271/2008-01-1171

Hu, X., Wen, S., Gao, Y., Xi, G., Khalighi, B., & Johnson, J. P. (2011). Experimental study on the effect of the shroud on the performance and flow field of an automotive cooling fan. *Proceedings of the Institution of Mechanical Engineers, Part D: Journal of Automobile Engineering*, *225*(5), 627–642. doi:10.1177/2041299110393179

Katoh, N., Ogawa, T., & Kuriyama, T. (1991). *Numerical simulation on the three dimensional flow and heat transfer in the engine compartment* (No. 910306). SAE Technical Paper. doi:10.4271/910306

Khaled, M., Harambat, F., & Peerhossaini, H. (2010). Temperature and heat flux behavior of complex flows in car underhood compartment. *Heat Transfer Engineering*, *31*(13), 1057–1067. doi:10.1080/01457631003640321

Lee, Y. L., & Hong, Y. T. (2000). Analysis of engine cooling including flow nonuniformity over a radiator. *International Journal of Vehicle Design*, *24*(1), 121–135. doi:10.1504/IJVD.2000.001877

Manna, S., & Kushwah, Y. S. (2015). *Optimization of a vehicle under hood airflow using 3D CFD Analysis* (No. 2015-01-0349). SAE Technical Paper. doi:10.4271/2015-01-0349

Mehravaran, M., & Zhang, Y. (2015). *Optimizing the geometry of fan-shroud assembly using CFD* (No. 2015-01-1336). SAE Technical Paper. doi:10.4271/2015-01-1336

Mou, B., He, B. J., Zhao, D. X., & Chau, K. W. (2017). Numerical simulation of the effects of building dimensional variation on wind pressure distribution. *Engineering Applications of Computational Fluid Mechanics*, *11*(1), 293–309. doi:10.1080/19942060.2017.1281845

Pan, F. P., Schoon, R., Putta, S., Ogale, A., & Chen, C. (2010). *A practical simulation approach for truck cooling system at early stage design process and development* (No. 2010-01-1927). SAE Technical Paper. doi:10.4271/2010-01-1927

Pang, S. C., Kalam, M. A., Masjuki, H. H., & Hazrat, M. A. (2012). A review on air flow and coolant flow circuit in vehicles' cooling system. *International Journal of Heat and Mass Transfer*, *55*(23-24), 6295–6306. doi:10.1016/j.ijheatmasstransfer.2012.07.002

Ramazanizadeh, M., Nazari, A. N., Ahmadi, M. H., & Chau, K. W. (2019). Experimental and numerical analysis of a nanofluidic thermosyphon heat exchanger. *Engineering*

Applications of Computational Fluid Mechanics, *13*(1), 40–47. doi:10.1080/19942060.2018.1518272

Shome, B., Kumar, V., Kumar, R. S. V., & Arora, G. (2006, July). *CFD prediction to optimize front end cooling module of a passenger vehicle*. Paper presented at International Refrigeration and Air Conditioning Conference, Purdue, US. Retrieved from https://docs.lib.purdue.edu/cgi/viewcontent.cgi?article = 1844&context = iracc

Soe, T. M., & Khaing, S. (2017). Comparison of turbulence models for computational fluid dynamics simulation of wind flow on Cluster of Buildings in Mandalay. *International Journal of Scientific and Research Publications*, *7*(8), 337–350.

Sofu, T., Chang, F. C., Dupree, R., Malipeddi, S., Uppuluri, S., & Shapiro, S. (2004). Measurement and analysis of underhood ventilation air flow and temperatures for an off-road machine. In *The aerodynamics of heavy vehicles: Trucks, buses, and trains* (pp. 373–383). Berlin: Springer.

Tai, C. H., Cheng, C. G., & Liao, C. Y. (2007). *A practical and simplified airflow simulation to assess underhood cooling performance* (No. 2007-01-1402). SAE Technical Paper. doi:10.4271/2007-01-1402

Taylor, D. O., & Chu, A. C. (1976). *Wind tunnel investigation of the effects of installation parameters on truck cooling system performance* (No. 760832). SAE Technical Paper. doi:10.4271/760832

Venter, S. J., & Kröger, D. G. (1992). The effect of tip clearance on the performance of an axial flow fan. *Energy Conversion and Management*, *33*(2), 89–97. doi:10.1016/0196-8904(92)90094-D

Yang, S., Wang, D., Dang, Y., & Li, L. (2015). *Numerical simulation and optimization of the underhood fluid field and cooling performance for heavy duty commercial vehicle under different driving conditions* (No. 2015-01-2902). SAE Technical Paper. doi:10.4271/2015-01-2902